A low-profile wideband circularly polarized metasurface antenna based on characteristic mode analysis

Kun Chai[1], Zhi Li[1], Yajuan Zhao[2], Liping Han[1] (iD), Guorui Han[1] (iD) and Yufeng Liu[1] (iD)

[1]School of Physics and Electronic Engineering, Shanxi University, Shanxi, China and [2]China-Belarus Belt and Road Joint Laboratory on Electromagnetic Environment Effect, No. 33 Research Institute of China Electronics Technology Group Corporation, Taiyuan, China

Abstract

A low-profile wideband circularly polarized (CP) metasurface antenna is demonstrated for C-band applications. The metasurface consists of 4×4 square patches with Z-shaped slots. Characteristic mode analysis is used to investigate the modal behavior of the metasurface, and a pair of degenerate modes is chosen as the operating modes. The CP radiation is realized by exciting a pair of degenerate modes of the metasurface through a slot antenna, which is used as a feed structure with a 90° phase difference. The CP bandwidth is further widened by combining the resonance modes of the metasurface and slot antenna. The measured results show that the −10 dB impedance bandwidth of the antenna is 3.47–4.76 GHz, and the 3 dB axial ratio bandwidth is 3.5–4.9 GHz with a peak gain of 6.9 dBic. Moreover, the antenna exhibits well left-hand CP radiation performances with a low profile of $0.046\lambda_0$.

CAMBRIDGE
UNIVERSITY PRESS

Introduction

Circularly polarized (CP) antennas have been widely utilized in wireless communication systems due to the strong anti-multipath interference and anti-fading ability [1, 2]. The traditional CP microstrip antennas have a simple structure, lightweight, and easiness of integration. However, due to the limited of narrow bandwidth, they are not suitable for applications with high transmission rates and high channel capacity. The bandwidth of the CP microstrip antennas can be improved by using thick dielectric substrates [3], stacked patches [4], and multi-feed networks [5]. However, the geometric dimension of the antennas will be increased.

Metamaterials have attracted much attention since their excellent characteristics of manipulating electromagnetic waves. As a two-dimensional metamaterial, metasurfaces have opened a new door to improve the performance of the conventional CP microstrip antenna [6–9]. Recently, some CP metasurface antennas have been reported. In papers [10, 11], a square metasurface is excited by a hybrid feed structure to obtain two degenerated orthogonal modes to realize CP radiation, and the axial ratio (AR) bandwidths (ARBWs) reach 14.5% and 20.9%, respectively. In paper [12], a nonuniform rectangular metasurface is fed by a slot antenna to radiate CP field. The ARBW is 17.43%. In paper [13], an S-shaped metasurface is proposed to efficiently covert linearly polarized into CP wave and the ARBW reaches 22%. In paper [14], an H-shaped metasurface is used as a radiator to form CP radiation. The ARBW is 14.3%. In addition, the metasurfaces can be used to improve the AR characteristic. In papers [15, 16], the CP radiation is realized through a patch antenna, and the ARBWs are increased up to 22.4% and 20.1% by loading patch and ring metasurfaces, respectively. For the aforementioned antennas, the biggest AR bandwidth is 22.4%, but the profile is $0.063\lambda_0$. Therefore, this work aims to design a low-profile wideband CP metasurface antenna.

In this paper, a low-profile wideband CP metasurface antenna is proposed. According to the characteristic mode analysis (CMA), two degenerate modes of the metasurface are chosen as the operating modes to realize the CP radiation. The metasurface is excited by a slot antenna. Combining the resonance modes of the slot antenna and metasurface to broaden CP bandwidth. The measured result shows that the −10 dB impedance bandwidth (IBW) of the proposed antenna is 3.47–4.76 GHz, and the 3 dB AR bandwidth (ARBW) is 3.5–4.9 GHz.

CMA of metasurface

Figure 1 shows the configuration of the proposed metasurface. It consists of 4×4 square patches with Z-shaped slots. The width of the unit cell is w_m, and the gap between the adjacent unit cells
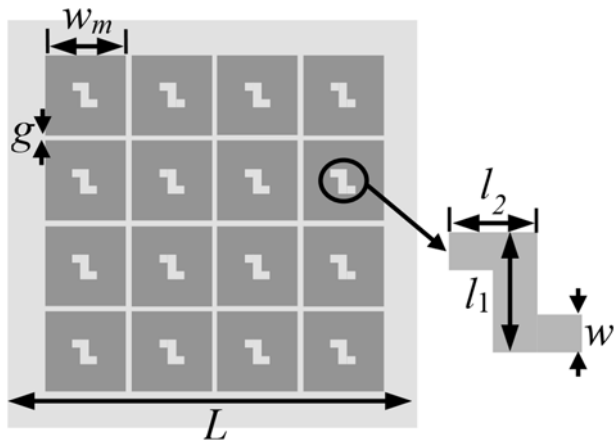
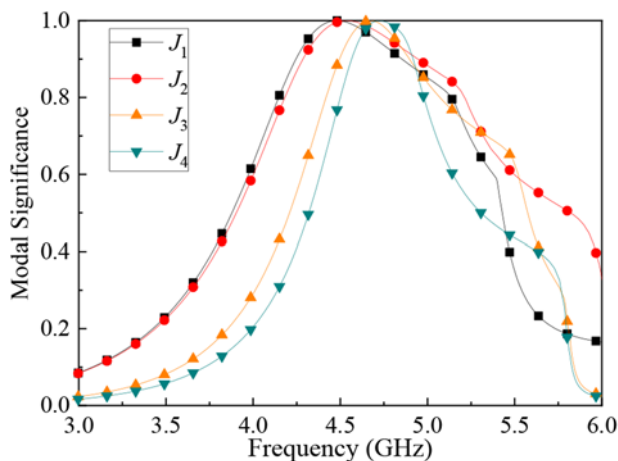**Figure 1.** Configuration of the metasurface.

Figure 2. Mode significance for the first four modes.

is g. The commercial simulation software CST 2019 is used to analyze the mode behaviors of the metasurface. The optimized

parameters are as follows: $L = 55$ mm, $w_m = 11$ mm, $g = 0.8$ mm, $l_1 = 2.6$ mm, $l_2 = 1$ mm and $w = 0.6$ mm, respectively.

The mode significance of the first four modes is given in Fig. 2. It is observed that the fundamental modes J_1/J_2 and high-order modes J_3/J_4 have the same frequency trend. The current distributions and radiation patterns of the first four modes are plotted in Fig. 3. It can be seen that the currents in modes J_1/J_2 is in-phase on the metasurface, but there is a 90° rotation. Hence, they are a pair of degenerate orthogonal modes, and good radiation patterns are obtained. Also, the currents in modes J_3/J_4 are self-symmetrical, and that a radiation null appears due to the out-of-phase current distributions. Figure 4 plots the characteristic angle of the first four modes. It can be seen that the phase difference between modes J_1/J_2 is 0°. According to the CP radiation mechanism, modes J_1/J_2 with equal amplitude are elected as operating modes, and the CP radiation can be obtained by using a feed structure with 90° phase difference.

Wideband CP metasurface antenna

To obtain CP radiation, an appropriate feed structure with a 90° phase difference should be employed to simultaneously excite J_1/J_2. As shown in Fig. 3, the maximum currents of modes J_1/J_2 concentrate at the central patches and the minor currents distribute at the surrounding patches. On the contrary, the maximum currents of modes J_3/J_4 are located at the four corners patches of the metasurface. Based on the above analysis, the feed structure should be positioned under the center patches of the metasurface, so that modes J_1/J_2 can be excited efficiently, while modes J_3/J_4 are difficult to be excited. A slot antenna is employed as the feed structure in this paper.

Figure 5 shows the configuration of the proposed antenna. It is composed of a metasurface aforementioned on the top substrate and a slot antenna on the bottom substrate. A stepped microstrip feedline is used to feed a tilted cross-slot on the ground plane. Both substrates have a relative dielectric constant of 4.4 and a loss tangent of 0.03. Numerical simulations are carried out using CST Microwave Studio. Following are the final optimized parameters of the antenna: $l_s = 24.4$ mm, $l_{s1} = 14.4$ mm, $w_s = 1.4$ mm, $l_f = 16$ mm, $w_f = 1.5$ mm, $l_{f1} = 16$ mm, $w_{f1} = 1$ mm,
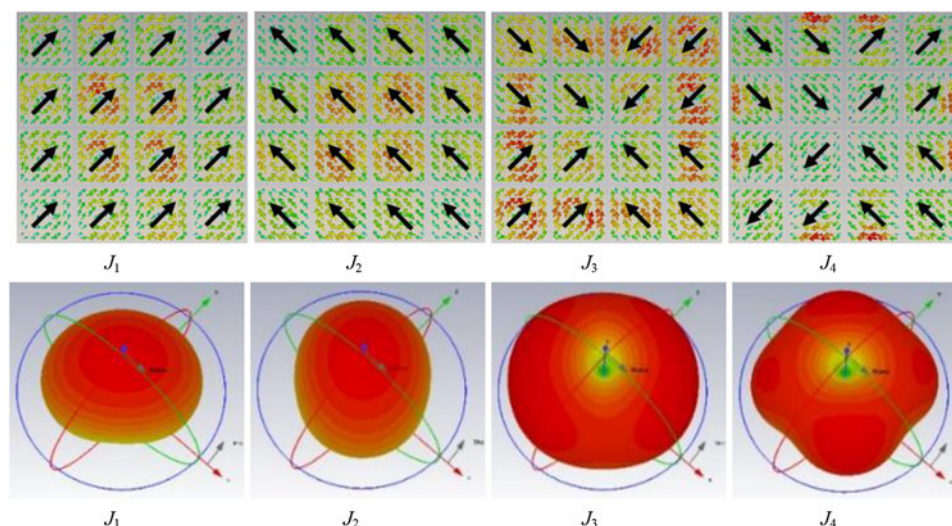

Figure 3. Current distributions and radiation patterns for J_1 and J_2 at 4.3 GHz, and J_3 and J_4 at 4.75 GHz.
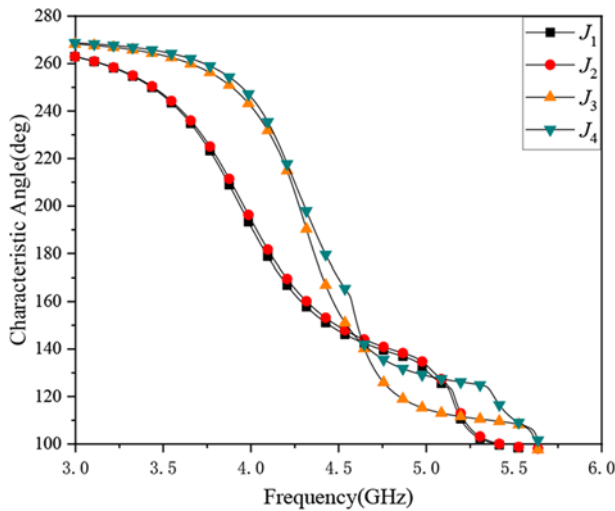
Figure 4. Characteristic angle for the first four modes.

$h_1 = 3.2$ mm, and $h_2 = 0.8$ mm, respectively. The S_{11} and AR of the antenna with/without the metasurface are depicted in Fig. 6. It is observed that the slot antenna without the metasurface has a -10 dB IBW of 6.79% (4.51–4.83 GHz), and a 3 dB ARBW of 3.44% (4.57–4.73 GHz). When the metasurface is loaded, the IBW of the antenna is 30.54% (3.44–4.68 GHz), and the ARBW is 28.43% (3.56–4.74 GHz). By combining the resonance modes

of the metasurface and slot antenna, the wideband CP radiation is achieved.

To illustrate the CP mechanism, the surface current distribution of the metasurface at 4.3 GHz and the slot antenna at 4.65 GHz are illustrated in Fig. 7. It can be seen that the current at both 4.3 and 4.65 GHz rotates in the clockwise direction for different phases. As a result, the left-hand CP radiation is formed.

The influences of the structural parameters on the antenna performance are also conducted. It is found that the metasurface element length w_m and the slot length l_{s1} play an important role. The S_{11} and AR for different w_m are given in Fig. 8. It can be seen that w_m mainly affects the AR while the S_{11} are insensitive to w_m. When w_m increases from 10 to 11 mm, the ARBW is expanded from 4.55% (4.3–4.5 GHz) to 27.54% (3.6–4.75 GHz). The CP performance deteriorates when w_m reaches up to 12 mm. Figure 9 shows the S_{11} and AR with different l_{s1}. It is observed that, when l_{s1} increases from 13.4 to 14.4 mm, both the IBW and ARBW increase. When l_{s1} reaches up to 15.4 mm, the IBW increases while the ARBW decreases.

Measurement results and discussions

To demonstrate the performance of the proposed antenna, a prototype of the antenna is fabricated and measured, as shown in Fig. 10. The S_{11} is measured by an Agilent N5221A vector network analyzer, and the far-field radiation performance, which contains the AR, gain, and radiation patterns, is measured by using a Lab-Volt 8092 antenna training and measuring system in a microwave anechoic chamber.
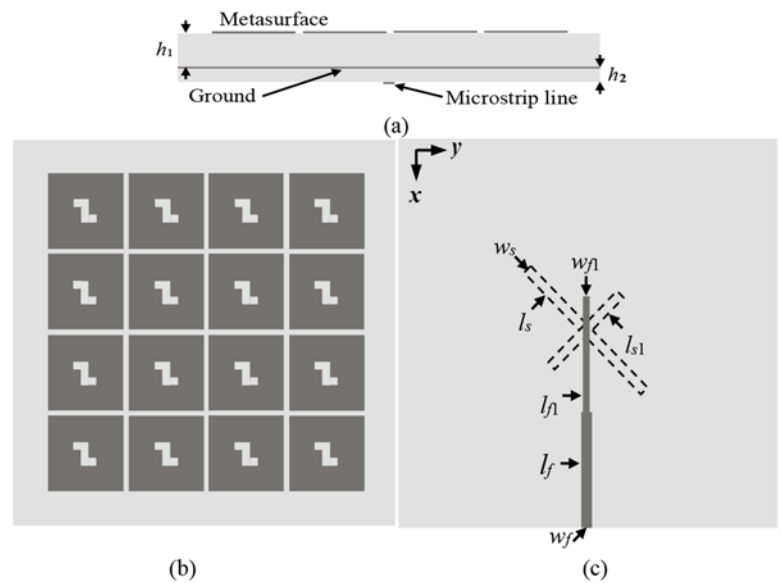

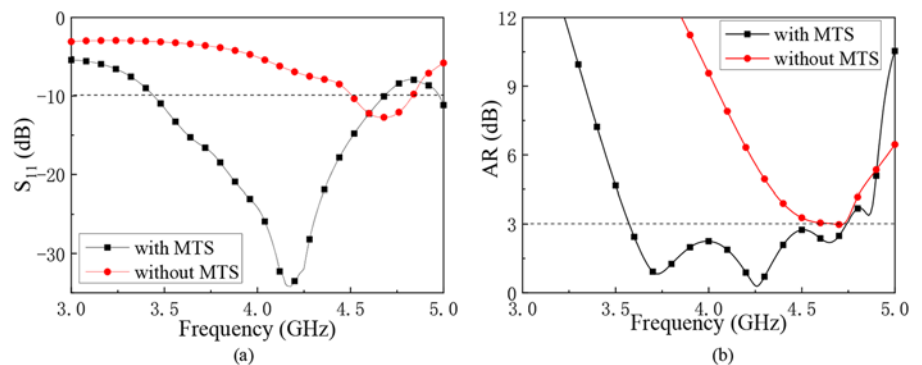**Figure 5.** Configuration of the antenna, (a) side view; (b) top view; (c) bottom view.

Figure 6. Simulated results of the antenna with or without the metasurface, (a) S_{11}; (b) AR.
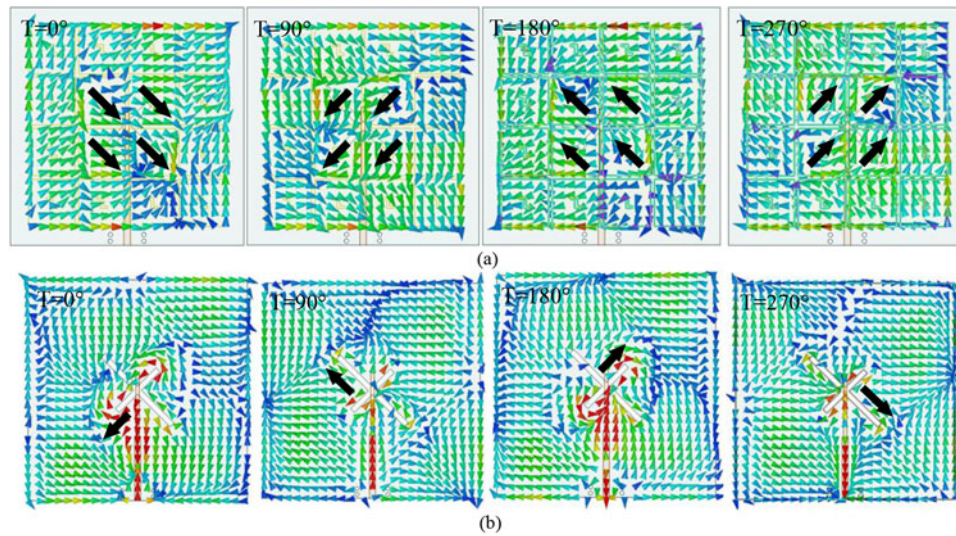
Figure 7. Surface current distributions on the metasurface and the slot antenna, (a) metasurface at 4.3 GHz; (b) slot antenna at 4.65 GHz.
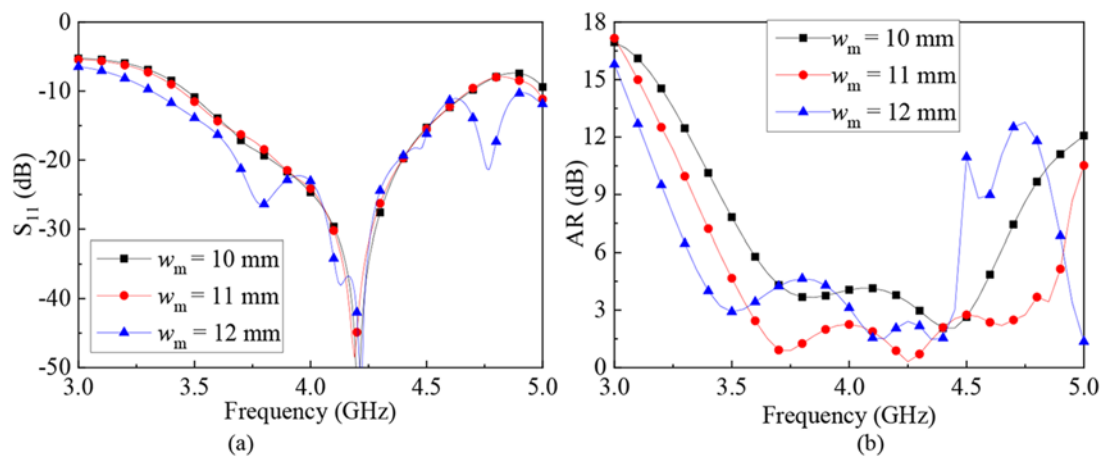

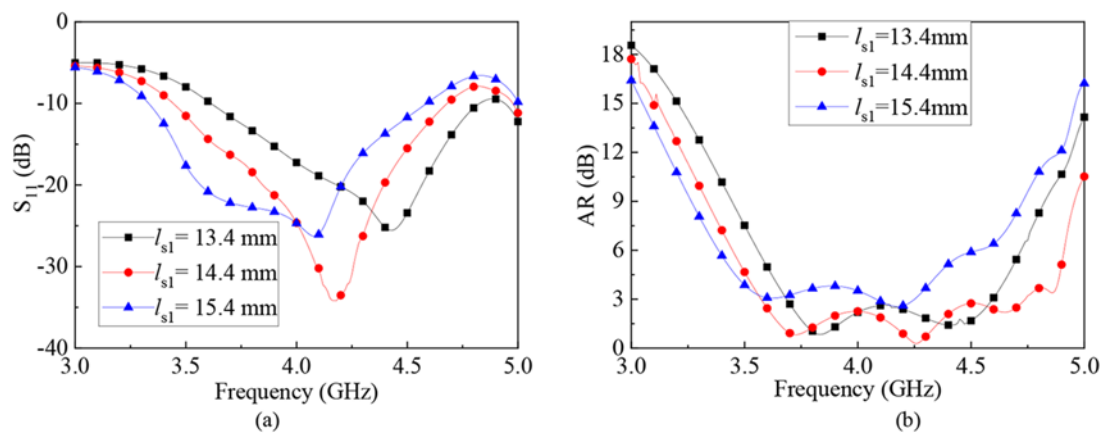**Figure 8.** S_{11} and AR for different w_m, (a) S_{11}, (b) AR.

Figure 9. S_{11} and AR for different l_{s1}, (a) S_{11}, (b) AR.
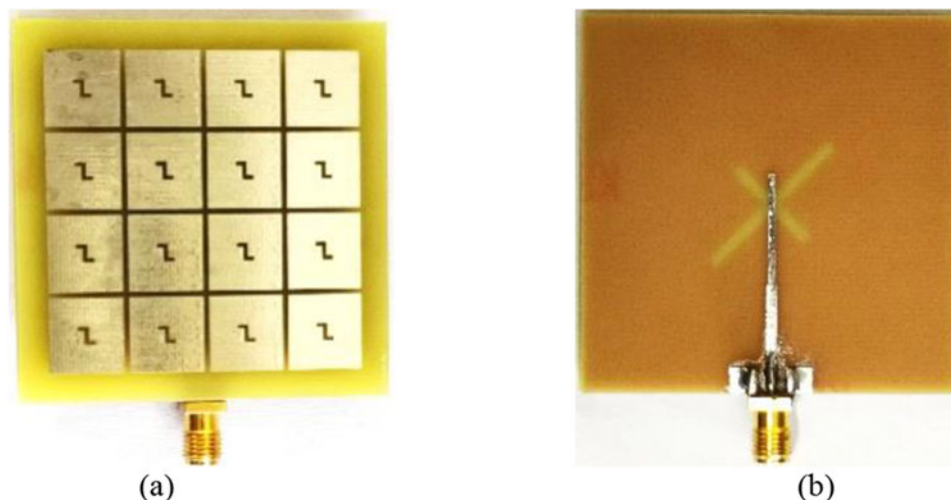
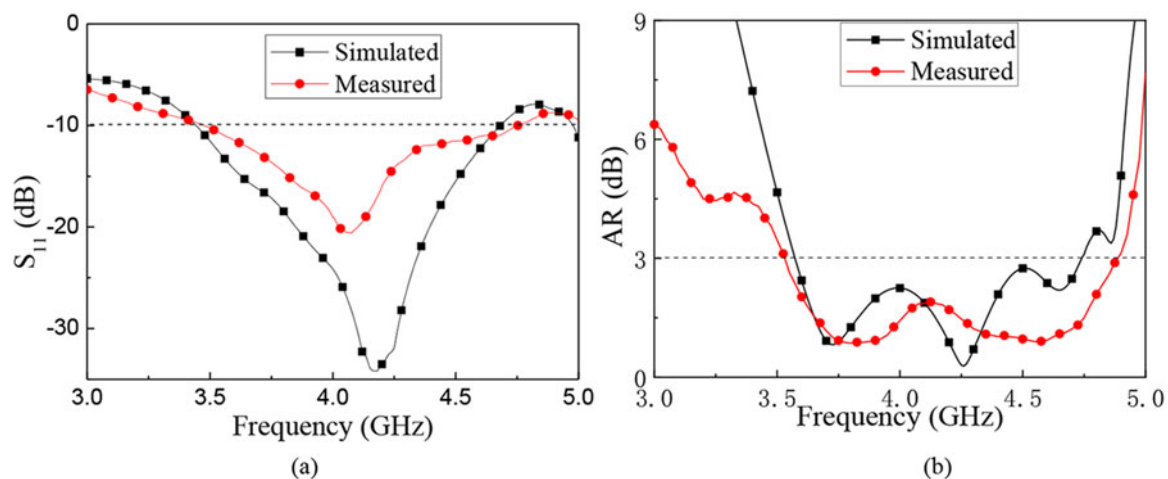**Figure 10.** Photograph of the antenna, (a) top view; (b) back view.

Figure 11. Simulated and measured results of the antenna, (a) S_{11}; (b) AR.

Figure 11 plots the measured and simulated S_{11} and AR of the antenna. It can be seen that reasonable agreement between the simulation and measurement results is obtained. The simulated and measured −10 dB IBW is 30.5% (3.44–4.68 GHz) and 31.3% (3.47–4.76 GHz), respectively. The simulated and measured 3 dB ARBW is 28.4% (3.56–4.74 GHz) and 33.3% (3.5–4.9 GHz), respectively. The discrepancy is mainly caused by the deviation of the dielectric constant and the effect of the subminiature version A (SMA) connector.

The simulated and measured far-field radiation patterns in *xoz* and *yoz* planes are plotted in Fig. 12. It is obvious that the proposed antenna realizes the left-hand CP radiation along +*z*-direction in the operating bandwidth. Figure 13 shows the simulated and measured antenna gains varying as frequency. The measured peak gain in the CP bandwidth reaches 6.9 dBic. It is noted that the gain after

4.25 GHz decreases, which is caused by the increasing right-hand CP component.

Finally, a performance comparison of the reported and proposed CP metasurface antennas is provided in Table 1. It is obvious that the size of proposed antenna is the smallest except [13]. Compared to the antenna in literature [13], the antenna in this work has a wider AR bandwidth.

Conclusion

A low-profile wideband CP metasurface antenna has been demonstrated experimentally. The modes behavior of the metasurface is investigated by the CMA, and two required degenerate modes of the metasurface are excited by the slot antenna to generate CP radiation. Combined with the resonance mode of the slot antenna
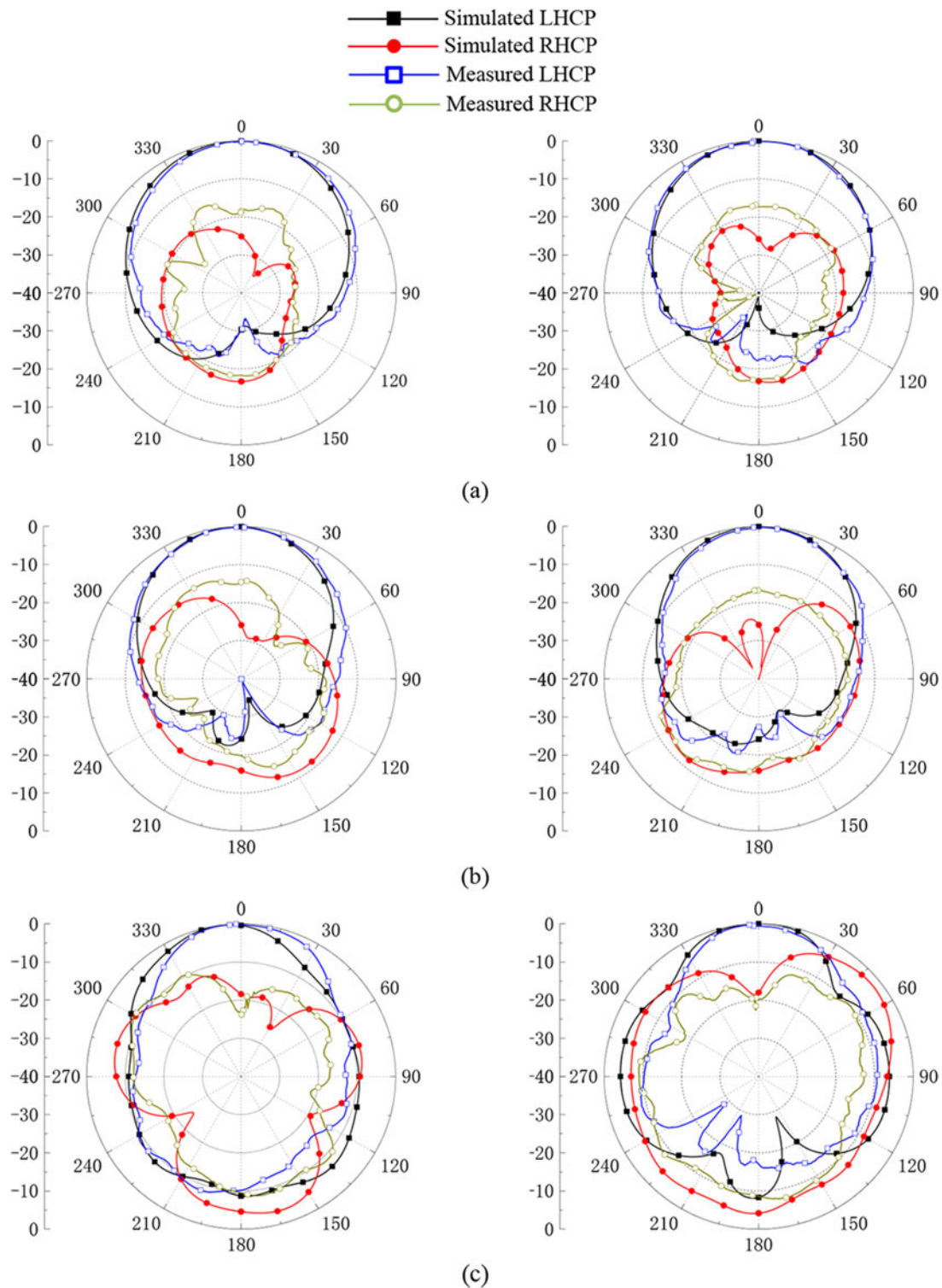
Figure 12. Normalized radiation patterns in *xoz* plane (left side) and *yoz* plane (right side), (a) at 3.75 GHz; (b) at 4.2 GHz; (c) at 4.65 GHz.

and metasurface, broadband CP radiation is realized. The fabricated antenna with a low profile of $0.046\lambda_0$ exhibits a measured wide −10 dB IBW of 31.3% (3.47–4.76 GHz) and a 3 dB ARBW of

33.3% (3.5–4.9 GHz), respectively. The overlapping CP bandwidth can cover the C-band downlink spectrum, and the simple design can be easily integrated into the communication devices.
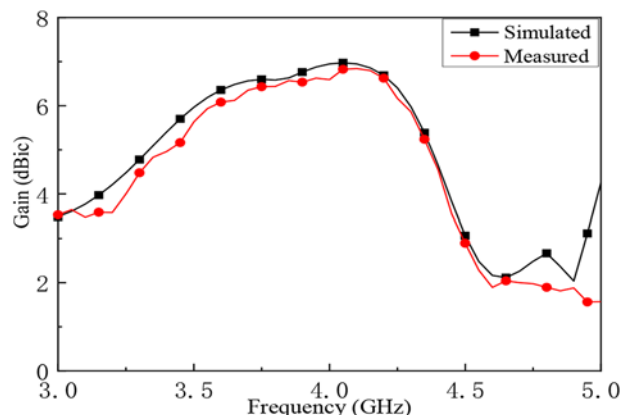
Figure 13. Gains of the antenna.

Table 1. Performance of CP metasurface antennas

Ref.	Size (λ_0^3)	Fre. (GHz)	IBW (%)	ARBW (%)
[10]	$0.93 \times 0.93 \times 0.024$	1.4	17	14.5
[11]	$1 \times 1 \times 0.07$	5.5	28.2	20.9
[12]	$0.72 \times 0.72 \times 0.068$	2.15	16.67	17.43
[13]	$0.48 \times 0.48 \times 0.057$	5.9	43.22	22
[14]	$1.3 \times 1.3 \times 0.067$	5.2	38.8	14.3
[15]	$0.86 \times 0.86 \times 0.063$	4.75	34.7	22.4
[16]	$1.1 \times 1.1 \times 0.093$	27.5	34.7	20.1
Proposed	$0.64 \times 0.64 \times 0.046$	3.5	31.3	33.3

Competing interest. The authors report that they have no known conflict of interests or personal relationships that could have appeared to influence the work reported in this paper.

Author contributions. Kun Chai and Zhi Li performed the simulations, Professor Liping Han guided the design, Yajuan Zhao, Guorui Han, and Yufeng Liu provided support during the experiment. All authors contributed equally to analyzing data and reaching conclusions, and in writing the paper.

References

1. **Cao R and Yu S-C** (2015) Wideband compact CPW-fed circularly polarized antenna for universal UHF RFID reader. *IEEE Transactions on Antennas and Propagation* **63**, 4148–4151.
2. **Dash SKK, Khan T and Kanaujia B** (2018) Circularly polarized dual facet spiral fed compact triangular dielectric resonator antenna for sensing applications. *IEEE Sensors Letters* **2**, 1–4.
3. **Kovitz JM and Rahmat-Samii Y** (2014) Using thick substrates and capacitive probe compensation to enhance the bandwidth of traditional CP patch antennas. *IEEE Transactions on Antennas and Propagation* **62**, 4970–4979.
4. **Esselle KP and Verma AK** (2017) Wideband circularly polarized stacked microstrip antennas. *IEEE Antennas and Wireless Propagation Letters* **6**, 21–24.
5. **Targonski SD and Pozar DM** (1993) Design of wideband circularly polarized aperture-coupled microstrip antennas. *IEEE Transactions on Antennas and Propagation* **41**, 214–220.
6. **Juan Y, Yang WC and Che WQ** (2019) Miniaturized low-profile circularly polarized metasurface antenna using capacitive loading. *IEEE Transactions on Antennas and Propagation* **67**, 3527–3532.
7. **Nasimuddin N, Chen ZN and Qing XM** (2016) Bandwidth enhancement of a single-feed circularly polarized antenna using a metasurface: Metamaterial-based wideband CP rectangular microstrip antenna. *IEEE Antennas and Propagation Magazine* **58**, 39–46.
8. **Ta SX and Par I** (2015) Low-profile broadband circularly polarized patch antenna using metasurface. *IEEE Transactions on Antennas and Propagation* **63**, 5929–5934.
9. **Pan YM, Hu PF, Zhang XY and Zheng SY** (2016) A low-profile high-gain and wideband filtering antenna with metasurface. *IEEE Transactions on Antennas and Propagation* **64**, 2010–2016.
10. **Liu SH, Yang DQ and Pan J** (2019) A low-profile circularly polarized metasurface antenna with wide axial-ratio beamwidth. *IEEE Antennas and Wireless Propagation Letters* **18**, 1438–1442.
11. **Gao X, Tian GW, Shou ZY and Li SM** (2021) A low-profile broadband circularly polarized patch antenna based on characteristic mode analysis. *IEEE Antennas and Wireless Propagation Letters* **20**, 214–218.
12. **Dicandia F and Genovesi S** (2020) Characteristic modes analysis of non-uniform metasurface superstrate for nanosatellite antenna design. *IEEE Access* **8**, 176050–176061.
13. **Supreeyatitikul N, Lertwiriyaprapa T and Phongcharoenpanich C** (2021) S-shaped metasurface-based wideband circularly polarized patch antenna for C-band applications. *IEEE Access* **9**, 23944–23955.
14. **Zhao C and Wang CF** (2018) Characteristic mode design of wide band circularly polarized patch antenna consisting of H-shaped unit cells. *IEEE Access* **6**, 25292–25299.
15. **Yang HC, Liu XY and Adisaputra A** (2020) Wideband circularly polarized antenna with all-textile metasurface for off-body communications. In *2020 9th Asia-Pacific Conference on Antennas and Propagation (APCAP)*, 1–2.
16. **Hussain N, Jeong MJ, Abbas A, Kim TJ and Kim N** (2020) A metasurface-based low-profile wideband circularly polarized patch antenna for 5G millimeter-wave systems. *IEEE Access* **8**, 22127–22135.

Kun Chai received the B.S. degree in electronic and Information Engineering from Shanxi University, Taiyuan, China, in 2019. Currently, he is a graduate in Shanxi University, Taiyuan, China. His research interests include design and analysis of circularly polarized antenna.
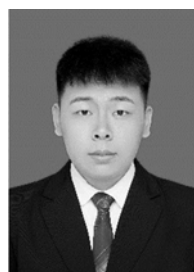
Zhi Li received the B.S. degree in electronic and Information Engineering from Taiyuan Normal University, Taiyuan, China, in 2019. Currently, he is a graduate in Shanxi University, Taiyuan, China. His research interests include design and analysis of metasurface antenna.
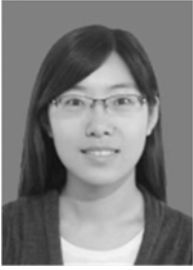
Yajuan Zhao received the M.S. degrees in communication engineering from Shanxi University, Taiyuan, China, in 2014. Currently, she is an engineer at the No. 33 Research Institute of China Electronics Technology Group Corporation. Her research interests include electromagnetic shielding composite materials, transparent stealth metamaterials, and metamaterials structure function integration.

Liping Han received the B.S., M.S., and Ph.D. degrees in electronic engineering from Shanxi University, Taiyuan, China, in 1993, 2002, and 2010, respectively. Currently, she is working as an associate professor with the School of Physics and Electronic Engineering, Shanxi University. Her research interests include microwave and millimeter-wave integrated circuits and microstrip antenna.
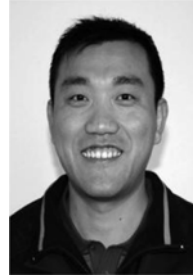
Guorui Han was born in Shanxi Taiyuan, China, in 1977. He received the B.S. and M.S. degrees in Applied Mechanics from Peking University, Beijing, China, in 2000 and 2004, respectively. He received the Ph.D. degree in Radio Physics from Shanxi University, Taiyuan, China, in 2013. Currently, he is working as an associate professor in School of Physics and Electronic Engineering, Shanxi University. His research interests include microwave and millimeter-wave antenna and MIMO antenna.

Yufeng Liu was born in Shanxi Lv liang, China, in 1986. He received the Ph.D. degree in radio physics from Sichuan University, Sichuan, China, in 2014. In 2015, he joined the College of Physics and Electronic Engineering, Shanxi University. His research is mainly focused on computational electromagnetics and antenna design.